

# Mid-infrared dual-comb spectroscopy of volatile organic compounds across long open-air paths

GABRIEL YCAS<sup>1,2</sup>, FABRIZIO R. GIORGETTA<sup>1,2\*</sup>, KEVIN C. COSSEL<sup>1</sup>, ELEANOR M. WAXMAN<sup>1</sup>, ESTHER BAUMANN<sup>1,2</sup>, NATHAN R. NEWBURY<sup>1</sup>, AND IAN CODDINGTON<sup>1</sup>

<sup>1</sup>National Institute of Standards and Technology, Boulder, Colorado 80305, USA

<sup>2</sup>Department of Physics, University of Colorado, Boulder, Colorado 80309, USA

\*Corresponding author: [fabrizio@nist.gov](mailto:fabrizio@nist.gov)

Compiled December 17, 2018

Open-path measurements of atmospheric gas species in the air including volatile organic compounds are essential to quantify emissions from sources like oil and gas, forest fires and industry. Here, we extend open-path dual-comb spectroscopy to probe the fundamental mid-infrared C-H stretch modes of volatile organic compounds over up to 1 km long open-air paths. The spectrometer's high resolution and accuracy facilitates suppression of strong spectral clutter from atmospheric water and methane, allowing quantitative measurements of released acetone and isopropanol with a  $1\text{-}\sigma$  sensitivity of 5.7 ppm·m respectively 2.4 ppm·m, and of ambient atmospheric ethane with a  $1\text{-}\sigma$  sensitivity of 0.4 ppb, measured with 1 minute time resolution over hours. These results underline the potential of dual-comb spectroscopy for quantifying emissions.

Work of the US government, not subject to copyright.

<http://dx.doi.org/10.1364/optica.XX.XXXXXX>

Volatile organic compounds (VOCs) play an important role in contributing to ozone and aerosol formation in the atmosphere [1–3]. Open-path measurements of atmospheric VOCs are important for quantifying emissions from sources as diverse as forest fires [4], oil and gas operations [2, 5] and industrial plants [6]. To date, the primary measurement technique available has been open-path Fourier transform infrared spectroscopy (OP-FTIR) [7, 8]. While the broad spectral coverage of OP-FTIR enables the measurement of many species, its usually low resolution and a changing instrument lineshape result in low absolute accuracy of the retrieved concentration [9]. In addition, the typical OP-FTIR black-body light source limits path lengths to at most several hundred meters in order to maintain a sufficient

signal-to-noise ratio. Here, we demonstrate an alternative technique, mid-infrared (MIR) dual-comb spectroscopy (DCS), and use it to measure multiple VOCs, namely released acetone and isopropanol and ambient ethane ( $\text{C}_2\text{H}_6$ ), over up to 1 km long open-air paths.

In the near-infrared (NIR), open-path DCS has emerged as a promising measurement technique for the quantification of industrial releases such as methane emissions from oil and gas operations [10, 11] or city-wide traffic emissions [12]. This is driven by the broad spectral coverage, fast acquisition times, high spectral resolution and negligible instrument lineshape possible with DCS [13], which enables multi-species detection with low sensitivity to turbulent air paths [14] and calibration-free, sub-percent-level agreement in retrieved concentrations between multiple systems [15]. However, these systems have been limited to quantifying molecules with part-per-million (ppm) level concentrations. To look for the more rarefied VOCs or other industrial pollutants it is necessary to extend past the weak overtone transitions of the NIR and access fundamental vibrational transitions further in the infrared, which can be 1000 times stronger. While there have been many DCS demonstrations in the MIR region, covering atmospheric transmission windows at  $2000\text{ cm}^{-1} - 3300\text{ cm}^{-1}$  [16–22] and  $750\text{ cm}^{-1} - 1250\text{ cm}^{-1}$  [23–27], these experiments have been limited to inside the laboratory or few-meter-scale outdoor paths, despite their importance for a variety of sensing applications.

Here we present MIR DCS over paths of up to 1 km. Spectral clutter from atmospheric water and methane is strongly suppressed by subtracting a lineshape-based model. With a broad comb spectrum spanning from  $2750\text{ cm}^{-1}$  to  $3150\text{ cm}^{-1}$ , we show detection not only of small molecules but also of larger, more broadly absorbing VOCs such as acetone and isopropanol that do not have rovibrationally-resolved lines under atmospheric conditions.  $\text{C}_2\text{H}_6$ , a small hydrocarbon, was detected at atmospheric background part-per-billion (ppb) levels across a 1 km open-air path. As in previous open-path NIR spectroscopy [14, 15], we combine both combs before propagation across the turbulent air path so that turbulence-driven phase front distortions are common mode. This eliminates turbulence-induced phase noise and retains high heterodyne mixing efficiency be-

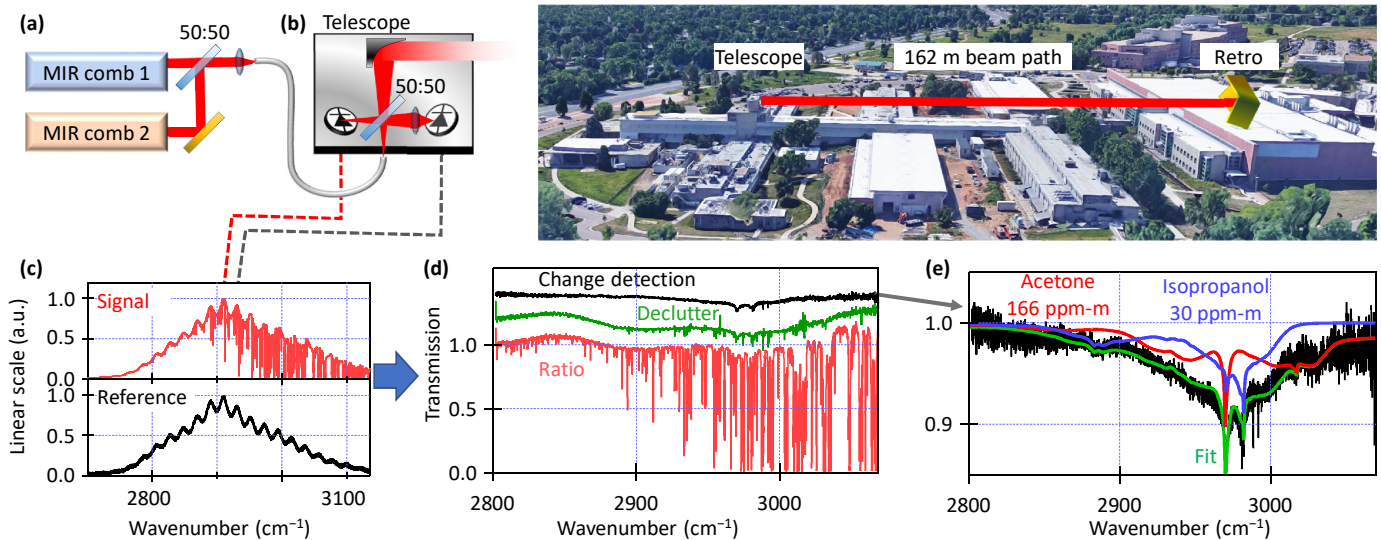


**Fig. 1.** Overview. (a) Two MIR frequency combs are generated with a dual-branch difference frequency generation scheme [21]. Both combs are phase stabilized by locking the carrier-envelope offset frequency and locking to a common cavity-stabilized continuous-wave (CW) laser at 1560 nm. (b) Telescope transceiver and Satellite image of the open-air link to a corner cube retroreflector (Imagery: Google). The reflected light is collected by the same telescope using a 50:50 beamsplitter. (c) Typical spectra measured on signal and reference detectors. (d) Intermediate spectral processing steps, with declutter and change detection spectra offset for clarity. (e) Expanded view of the change detection spectrum. The remaining structure is mostly absorption from the released gases. A fitted model (acetone and isopropanol) is shown in green and constituent components are shown in red and blue. The displayed data is averaged for 1 minute and smoothed from  $0.0067 \text{ cm}^{-1}$  (200 MHz) to  $0.067 \text{ cm}^{-1}$  resolution. For declutter and change detection spectra, points where the clutter transmission drops below 0.2 are masked out.

tween the combs.

In the first set of experiments, controlled combinations of VOCs are released by evaporation from two  $\sim 0.08 \text{ m}^2$  surface area trays, one containing acetone and the other isopropanol. These trays are placed just underneath the optical path so that the plume intersects the beam under most wind conditions. By adding and removing the trays, time-varying plumes of the two VOCs are produced. Path-integrated spectra are recorded continuously during this period.

The spectrometer setup is shown in Fig. 1(a–b) and includes the MIR dual-comb spectrometer described in [21] and a telescope to transmit and collect light over the open-air path. The spectrometer consists of two 200 MHz repetition rate MIR frequency combs, each generated using difference-frequency generation in a bulk periodically-poled lithium niobate (PPLN) crystal from a polarization-maintaining erbium fiber frequency comb [28]. The two MIR combs are combined on a 50:50 beamsplitter, and 5 mW of light from each comb are coupled into a single-mode  $\text{ZrF}_4$  fiber for transmission to the telescope. At the telescope, the MIR light diverges from the fiber tip, passes through a second 50:50 beamsplitter, and is collimated by a 100 mm diameter off-axis parabolic mirror with an effective focal length of 179 mm. This results in a launched beam diameter of  $\sim 75 \text{ mm}$ . An optical link is established between the telescope and a remote 63.5 mm diameter retroreflector, with the returned light collected by the same telescope. The 50:50 beamsplitter picks off half of the outgoing light for the reference channel and half of the returned light for the signal channel. Thermoelectrically cooled 100 MHz bandwidth HgCdTe detectors record the light (interferograms) on each channel. Interferograms repeat every 10 ms (given by the 100 Hz difference in comb repetition rates) and consecutive interferograms are coherently averaged for 1 minute

in a field-programmable gate array (FPGA) before being saved to disk [21]. The averaged interferograms are then Fourier transformed to obtain spectra. The achieved DCS figure-of-merit is  $1.2 \times 10^6$  [13].

The measured spectra are processed as shown in Fig. 1(c–e). First, the signal spectrum is divided by the reference spectrum to remove comb structure and create the ratio spectrum (red trace in Fig. 1(d)). Next, spectral clutter is suppressed by dividing out interfering atmospheric species. To do this an atmospheric transmission model using Voigt lineshape parameters from the Hitran 2016 database [29] is fitted to and then divided from the ratio spectrum, giving the green trace in Fig. 1(d). This decluttering not only cleans up the spectrum, but also extracts absolute concentrations of atmospheric species [14], including water ( $\text{H}_2\text{O}$ ), semiheavy water ( $\text{HDO}$ ),  $\text{H}_2^{18}\text{O}$ , and methane ( $\text{CH}_4$ ). For both the decluttering and these retrievals, the high resolution, wavenumber accuracy, and negligible lineshape of DCS is essential, as atmospheric  $\text{H}_2\text{O}$  and  $\text{CH}_4$  absorption lines are  $\sim 0.1 \text{ cm}^{-1}$  wide.

Even after removal of the reference spectrum and decluttering, additional spectral structure remains. For detection of controlled chemical releases, this baseline structure can be suppressed by change detection, in which we ratio all spectra with a spectrum acquired before the release. With change detection, extracted gas concentrations are relative to the concentrations present in the pre-release spectrum.

Finally, the processed spectrum is fitted with a model containing a linear baseline and isopropanol and acetone reference spectra from the Pacific Northwest National Laboratory (PNNL) database [30]. Figure 2 shows extracted dry concentrations by volume for a 3 hour measurement across the 162 m open-air link. At 14:08, the tray containing acetone is positioned under

the beam path. The measured path-integrated concentration increases to around 150 ppm-m, with strong variability caused by atmospheric mixing of the evaporating acetone fumes. At 14:45, the second tray filled with isopropanol is added, leading to an isopropanol concentration of around 25 ppm-m. After first removing the acetone tray at 15:14 and then the isopropanol tray at 16:00, the measured concentrations drop back to zero, but show stronger variability than before the solvent releases. The reason for this is not clear, but possible causes are residual VOC fumes and slow temporal variations in spectral baseline. It is assumed that no acetone and isopropanol was present prior to 14:00 and a 7 minute data set starting at 13:18 is used as the pre-release spectrum for change detection.

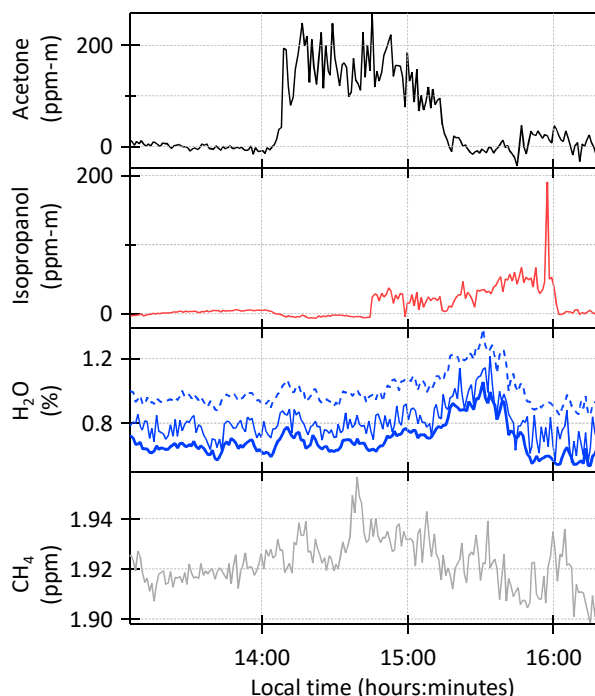


**Fig. 2.** 3 hour measurement across the 162 m open-air path with 1 minute time resolution. Acetone is added at 14:08 and removed at 15:14. Isopropanol is added just before 14:45 and removed at 16:00. The isopropanol spike just before 16:00 is caused by an accidental spill of isopropanol. The bottom two panels show absolute concentrations of atmospheric water isotopes  $\text{H}_2^{16}\text{O}$  bold solid,  $\text{H}_2^{18}\text{O}$  solid (offset by 0.2%), and  $\text{HD}^{16}\text{O}$  dashed (offset by 0.4%), all scaled with the isotopic abundances used in Hitran ( $\text{H}_2^{16}\text{O}$ : 0.997317,  $\text{H}_2^{18}\text{O}$ : 0.002,  $\text{HD}^{16}\text{O}$ :  $3.718840 \times 10^{-4}$ ) and  $\text{CH}_4$ .

As the background level of acetone and isopropanol can be safely assumed to be well below the instrument sensitivity, the DCS sensitivity is estimated as the standard deviation of concentration levels measured over a 3500 s time span before the initial release at 14:08. The obtained 1- $\sigma$  sensitivities for 1 minute averaging are 5.7 ppm-m for acetone and 2.4 ppm-m for isopropanol. The Allan deviation is below 2 ppm-m for acetone and below 1 ppm-m for isopropanol for averaging times from 100 s to 800 s. Here, DCS sensitivity is limited by residual baseline fluctuations in the retrieved spectra. Laboratory experiments suggest that they are caused in part by changes in the optical path through the telescope, coupled to the spatial illumination of the detector. Future work should consider more sophisticated telescope

designs for more uniform detector illumination.

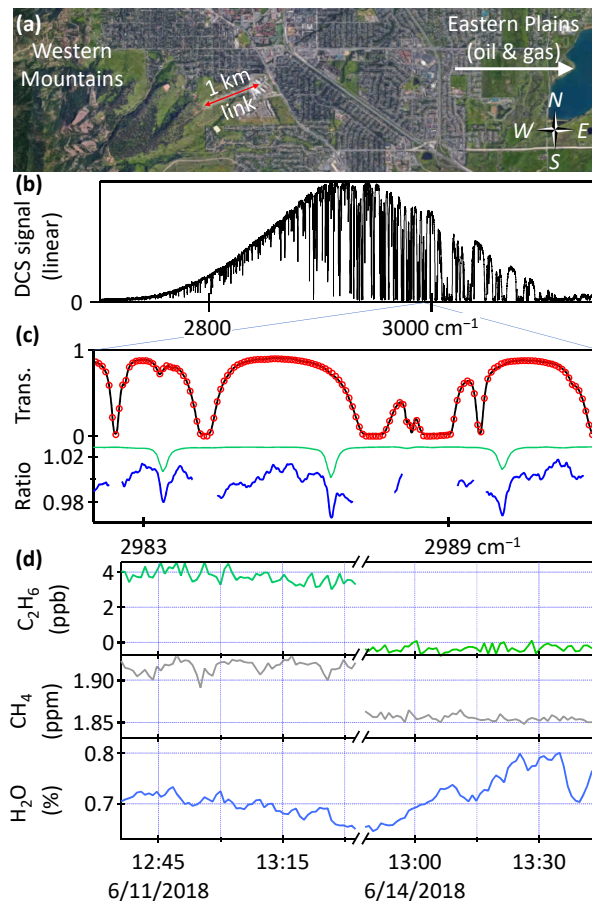


**Fig. 3.** 1 km open-air link. (a) Satellite image showing the 1 km DCS open path on the NIST campus in Boulder, Colorado (Imagery: Google).; (b) raw DCS spectrum showing strong atmospheric clutter; (c) close-up of 6/11/2018 DCS transmission spectrum averaged over 1 hour and smoothed to  $0.067 \text{ cm}^{-1}$  resolution (black) along with a fitted model including water and methane (red circles). The ratio (blue) of DCS spectrum and model clearly shows  $\text{C}_2\text{H}_6$  features, as seen when comparing to the PNNL  $\text{C}_2\text{H}_6$  reference transmission (green, 3.75 ppm). The ratio is masked at wavenumbers where the transmission drops below 0.2. (d) Extracted  $\text{C}_2\text{H}_6$ ,  $\text{CH}_4$  and  $\text{H}_2\text{O}$  concentrations acquired with 1 minute time resolution over two one-hour spans separated by three days. During easterly winds (6/11/2018 measurement), increased  $\text{CH}_4$  and  $\text{C}_2\text{H}_6$  concentrations are observed. The small negative offset in the 6/14/2018  $\text{C}_2\text{H}_6$  concentration is a systematic that is probably caused by baseline structure.

There are a large number of oil and gas extraction sites immediately east of the city of Boulder in the Denver-Julesburg (D-J) basin (and virtually none in the mountains to the west). As our measurement site is located just west of the D-J basin, we expect to measure increased levels of VOCs from oil and gas when the wind blows from the east, while lower background levels should be measured during westerly winds. Indeed, we detect enhancements of 3.75 ppb for  $\text{C}_2\text{H}_6$  and 60 ppb for  $\text{CH}_4$  during easterly winds. For this measurement, the path length was extended to 1 km (using a larger 127 mm-diameter retroreflector) as seen in Fig. 3(a), improving sensitivity to ambient gases at the cost of

increased spectral clutter from water and methane (Fig. 3(b)).

Change detection is no longer viable because  $C_2H_6$  and  $CH_4$  concentrations remain nearly constant during the 1 hour measurement span. Instead, open-path spectra are divided with a 'shorted path' spectrum taken with a retro reflector placed next to the telescope. The decluttered spectrum is generated as described above but, as is evident from Fig. 3(c), spectral structure at the 3% level remains. We attribute this residual structure to incomplete baseline removal, to spatial and temporal variations in atmospheric conditions (pressure, temperature, water content) across the path which are not accounted for in the model, to small inaccuracies in the Hitran 2016 lineshape parameters, and to deviations from the Voigt line shape [31] that are relevant for the saturated lines observed. Nevertheless, the ratio-ed spectrum in Fig. 3(c) clearly shows atmospheric  $C_2H_6$  absorption features.

By fitting a PNNL  $C_2H_6$  spectrum to the ratio-ed spectrum between  $2970\text{ cm}^{-1}$  and  $3003\text{ cm}^{-1}$ , path-averaged  $C_2H_6$  concentrations are extracted, as shown in Fig. 3(d) along with  $CH_4$  and  $H_2O$  concentrations. The average extracted  $C_2H_6$  concentration is 3.75 ppb with a statistical  $1-\sigma$  sensitivity of 0.4 ppb. This agrees with a  $C_2H_6$  point sensor located 10 km to the north-east that measured 3.5 ppb  $C_2H_6$  at that time. The average extracted  $CH_4$  concentration is 1872 ppb with a statistical  $1-\sigma$  sensitivity of 4 ppb. Also shown in Fig. 3(d) is a similar measurement performed three days later during westerly winds that shows no  $C_2H_6$  signature and 60 ppb lower  $CH_4$  concentrations. The ratio of  $C_2H_6$  to  $CH_4$  enhancement during easterly wind is 6%, consistent with oil and gas extraction being a significant source of hydrocarbon emissions in the D-J basin to the east of our measurement path [2, 5].

In conclusion, open-air mid-infrared dual-comb spectroscopy of acetone, isopropanol and of atmospheric ethane is presented. The high resolution and accuracy of DCS enables efficient spectral removal of interfering atmospheric species such as water and methane, which is crucial for detection of weak absorbers such as atmospheric ethane. This demonstrates the capabilities of MIR DCS as a sensitive multi-species open air detector, including chemical agents, precursors and pollutants with spectral signatures in cluttered regions and with broad, poorly featured absorption spectra. With even broader spectral coverage, similar performance should be achievable for other important hazardous pollutants such as benzene, toluene, ethylbenzene, and xylenes (BTEX).

**Funding.** DARPA defence sciences office (DSO), NIST.

**Acknowledgments.** We acknowledge comments on the manuscript from Pamela M. Chu and Adam J. Fleisher.

## REFERENCES

1. T. B. Ryerson, M. Trainer, J. S. Holloway, D. D. Parrish, L. G. Huey, D. T. Sueper, G. J. Frost, S. G. Donnelly, S. Schauffler, E. L. Atlas, W. C. Kuster, P. D. Goldan, G. Hübler, J. F. Meagher, and F. C. Fehsenfeld, *Science* **292**, 719 (2001).
2. G. Pétron, G. Frost, B. R. Miller, A. I. Hirsch, S. A. Montzka, A. Karion, M. Trainer, C. Sweeney, A. E. Andrews, L. Miller, J. Kofler, A. Bar-Ilan, E. J. Dlugokencky, L. Patrick, C. T. Moore, T. B. Ryerson, C. Siso, W. Kolodzey, P. M. Lang, T. Conway, P. Novelli, K. Masarie, B. Hall, D. Gunther, D. Kitzis, J. Miller, D. Welsh, D. Wolfe, W. Neff, and P. Tans, *J. Geophys. Res. Atmospheres* **117**, D04304 (2012).
3. J. L. Jimenez, M. R. Canagaratna, N. M. Donahue, A. S. H. Prevot, Q. Zhang, J. H. Kroll, P. F. DeCarlo, J. D. Allan, H. Coe, N. L. Ng, A. C. Aiken, K. S. Docherty, I. M. Ulbrich, A. P. Grieshop, A. L. Robinson, J. Duplissy, J. D. Smith, K. R. Wilson, V. A. Lanz, C. Hueglin, Y. L. Sun, J. Tian, A. Laaksonen, T. Raatikainen, J. Rautiainen, P. Vaattovaara, M. Ehn, M. Kulmala, J. M. Tomlinson, D. R. Collins, M. J. Cubison, E. J. Dunlea, J. A. Huffman, T. B. Onasch, M. R. Alfarra, P. I. Williams, K. Bower, Y. Kondo, J. Schneider, F. Drewnick, S. Borrmann, S. Weimer, K. Demerjian, D. Salcedo, L. Cottrell, R. Griffin, A. Takami, T. Miyoshi, S. Hatakeyama, A. Shimono, J. Y. Sun, Y. M. Zhang, K. Dzepina, J. R. Kimmel, D. Sueper, J. T. Jayne, S. C. Herndon, A. M. Trimborn, L. R. Williams, E. C. Wood, A. M. Middlebrook, C. E. Kolb, U. Baltensperger, and D. R. Worsnop, *Science* **326**, 1525 (2009).
4. V. Selimovic, R. J. Yokelson, C. Warneke, J. M. Roberts, J. de Gouw, J. Reardon, and D. W. T. Griffith, *Atmospheric Chem. Phys.* **18**, 2929 (2018).
5. J. Peischl, S. J. Eilerman, J. A. Neuman, K. C. Aikin, J. de Gouw, J. B. Gilman, S. C. Herndon, R. Nadkarni, M. Trainer, C. Warneke, and T. B. Ryerson, *J. Geophys. Res. Atmospheres* **123**, 7725 (2018).
6. W. F. Herget and J. D. Brasher, *Appl. optics* **18**, 3404 (1979).
7. T. L. Marshall, C. T. Chaffin, R. M. Hammaker, and W. G. Fateley, *Environ. science & technology* **28**, 224A (1994).
8. S. P. Levine and G. M. Russwurm, *TrAC Trends Anal. Chem.* **13**, 258 (1994).
9. L. Shao, W. Wang, P. R. Griffiths, and A. B. Leytem, *Appl. Spectrosc.* **67**, 335 (2013).
10. K. C. Cossel, E. M. Waxman, F. R. Giorgetta, M. Cermak, I. R. Coddington, D. Hesselius, S. Ruben, W. C. Swann, G.-W. Truong, G. B. Rieker, and N. R. Newbury, *Optica*, **4**, 724 (2017).
11. S. Coburn, C. B. Alden, R. Wright, K. Cossel, E. Baumann, G.-W. Truong, F. Giorgetta, C. Sweeney, N. R. Newbury, K. Prasad, I. Coddington, and G. B. Rieker, *Optica*, **5**, 320 (2018).
12. E. M. Waxman, K. C. Cossel, F. Giorgetta, G.-W. Truong, W. C. Swann, I. Coddington, and N. R. Newbury, *Atmospheric Chem. Phys. Discuss.* pp. 1–23 (2018).
13. I. Coddington, N. Newbury, and W. Swann, *Optica*, **3**, 414 (2016).
14. G. B. Rieker, F. R. Giorgetta, W. C. Swann, J. Kofler, A. M. Zolot, L. C. Sinclair, E. Baumann, C. Cromer, G. Petron, C. Sweeney, P. P. Tans, I. Coddington, and N. R. Newbury, *Optica*, **1**, 290 (2014).
15. E. M. Waxman, K. C. Cossel, G.-W. Truong, F. R. Giorgetta, W. C. Swann, S. Coburn, R. J. Wright, G. B. Rieker, I. Coddington, and N. R. Newbury, *Atmos. Meas. Tech.* **10**, 3295 (2017).
16. A. Schliesser, N. Picqué, and T. W. Hänsch, *Nat. Photonics* **6**, 440 (2012).
17. F. Zhu, A. Bicer, R. Askar, J. Bounds, A. A. Kolomenskii, V. Kelessides, M. Amani, and H. A. Schuessler, *Laser Phys. Lett.* **12**, 095701 (2015).
18. Z. Zhang, T. Gardiner, and D. T. Reid, *Opt. Lett.* **38**, 3148 (2013).
19. M. Yu, Y. Okawachi, A. G. Griffith, N. Picqué, M. Lipson, and A. L. Gaeta, *Nat. Commun.* **9**, 1869 (2018).
20. Y. Jin, S. M. Cristescu, F. J. M. Harren, and J. Mandon, *Appl. Phys. B* **119**, 1 (2015).
21. G. Ycas, F. R. Giorgetta, E. Baumann, I. Coddington, D. Herman, S. A. Diddams, and N. R. Newbury, *Nat. Photonics* **12**, 202 (2018).
22. A. V. Muraviev, V. O. Smolski, Z. E. Loparo, and K. L. Vodopyanov, *Nat. Photonics* **12**, 209 (2018).
23. A. Schliesser, M. Brehm, F. Keilmann, and D. van der Weide, *Opt. Express* **13**, 9029 (2005).
24. P. Jouy, J. M. Wolf, Y. Bidaux, P. Allmendinger, M. Mangold, M. Beck, and J. Faist, *Appl. Phys. Lett.* **111**, 141102 (2017).
25. O. Kara, L. Maidment, T. Gardiner, P. G. Schunemann, and D. T. Reid, *Opt. Express* **25**, 32713 (2017).
26. J. Westberg, L. A. Sterczewski, and G. Wysocki, *Appl. Phys. Lett.* **110**, 141108 (2017).
27. H. Timmers, A. Kowligy, A. Lind, F. C. Cruz, N. Nader, M. Silfies, G. Ycas, T. K. Allison, P. G. Schunemann, S. B. Papp, and S. A. Diddams, *Optica*, **5**, 727 (2018).
28. G.-W. Truong, E. M. Waxman, K. C. Cossel, E. Baumann, A. Klose, F. R. Giorgetta, W. C. Swann, N. R. Newbury, and I. Coddington, *Opt. Express* **24**, 30495 (2016).
29. I. E. Gordon, L. S. Rothman, C. Hill, R. V. Kochanov, Y. Tan, P. F. Bernath, M. Birk, V. Boudon, A. Campargue, K. V. Chance, B. J. Drouin, J. M. Flaud, R. R. Gamache, J. T. Hodges, D. Jacquemart, V. I. Perevalov, A. Perrin, K. P. Shine, M. A. H. Smith, J. Tennyson, G. C. Toon, H. Tran, V. G. Tyuterev, A. Barbe, A. G. Császár, V. M. Devi, T. Furtenbacher, J. J. Harrison, J. M. Hartmann, A. Jolly, T. J. Johnson, T. Karman, I. Kleiner, A. A. Kyuberis, J. Loos, O. M. Lyulin, S. T. Massie, S. N. Mikhailenko, N. Moazzen-Ahmadi, H. S. P. Müller, O. V. Naumenko, A. V. Nikitin, O. L. Polyansky, M. Rey, M. Rotger, S. W. Sharpe, K. Sung, E. Starikova, S. A. Tashkun, J. V. Auwera,

- G. Wagner, J. Wilzewski, P. Wcisło, S. Yu, and E. J. Zak, *J. Quant. Spectrosc. Radiat. Transf.* **203**, 3 (2017).
30. S. W. Sharpe, T. J. Johnson, R. L. Sams, P. M. Chu, G. C. Rhoderick, and P. A. Johnson, *Appl. Spectrosc.* **58**, 1452 (2004).
  31. C. D. Boone, K. A. Walker, and P. F. Bernath, *J. Quant. Spectrosc. Radiat. Transf.* **105**, 525 (2007).

## FULL REFERENCES

1. T. B. Ryerson, M. Trainer, J. S. Holloway, D. D. Parrish, L. G. Huey, D. T. Sueper, G. J. Frost, S. G. Donnelly, S. Schaubler, E. L. Atlas, W. C. Kuster, P. D. Goldan, G. Hübler, J. F. Meagher, and F. C. Fehsenfeld, "Observations of Ozone Formation in Power Plant Plumes and Implications for Ozone Control Strategies," *Science*. **292**, 719–723 (2001).
2. G. Pétron, G. Frost, B. R. Miller, A. I. Hirsch, S. A. Montzka, A. Karion, M. Trainer, C. Sweeney, A. E. Andrews, L. Miller, J. Kofler, A. Bar-Ilan, E. J. Dlugokencky, L. Patrick, C. T. Moore, T. B. Ryerson, C. Siso, W. Kolodzey, P. M. Lang, T. Conway, P. Novelli, K. Masarie, B. Hall, D. Guenther, D. Kitzis, J. Miller, D. Welsh, D. Wolfe, W. Neff, and P. Tans, "Hydrocarbon emissions characterization in the Colorado Front Range: A pilot study," *J. Geophys. Res. Atmospheres* **117**, D04304 (2012).
3. J. L. Jimenez, M. R. Canagaratna, N. M. Donahue, A. S. H. Prevot, Q. Zhang, J. H. Kroll, P. F. DeCarlo, J. D. Allan, H. Coe, N. L. Ng, A. C. Aiken, K. S. Docherty, I. M. Ulbrich, A. P. Grieshop, A. L. Robinson, J. Duplissy, J. D. Smith, K. R. Wilson, V. A. Lanz, C. Hueglin, Y. L. Sun, J. Tian, A. Laaksonen, T. Raatikainen, J. Rautiainen, P. Vaattovaara, M. Ehn, M. Kulmala, J. M. Tomlinson, D. R. Collins, M. J. Cubison, E. J. Dunlea, J. A. Huffman, T. B. Onasch, M. R. Alfarra, P. I. Williams, K. Bower, Y. Kondo, J. Schneider, F. Drewnick, S. Borrmann, S. Weimer, K. Demerjian, D. Salcedo, L. Cottrell, R. Griffin, A. Takami, T. Miyoshi, S. Hatakeyama, A. Shimono, J. Y. Sun, Y. M. Zhang, K. Dzepina, J. R. Kimmel, D. Sueper, J. T. Jayne, S. C. Herndon, A. M. Trimborn, L. R. Williams, E. C. Wood, A. M. Middlebrook, C. E. Kolb, U. Baltensperger, and D. R. Worsnop, "Evolution of Organic Aerosols in the Atmosphere," *Science* **326**, 1525–1529 (2009).
4. V. Selimovic, R. J. Yokelson, C. Warneke, J. M. Roberts, J. de Gouw, J. Reardon, and D. W. T. Griffith, "Aerosol optical properties and trace gas emissions by PAX and OP-FTIR for laboratory-simulated western US wildfires during FIREX," *Atmospheric Chem. Phys.* **18**, 2929–2948 (2018).
5. J. Peischl, S. J. Eilerman, J. A. Neuman, K. C. Aikin, J. de Gouw, J. B. Gilman, S. C. Herndon, R. Nadkarni, M. Trainer, C. Warneke, and T. B. Ryerson, "Quantifying Methane and Ethane Emissions to the Atmosphere From Central and Western U.S. Oil and Natural Gas Production Regions," *J. Geophys. Res. Atmospheres* **123**, 7725–7740 (2018).
6. W. F. Herget and J. D. Brasher, "Remote measurement of gaseous pollutant concentrations using a mobile Fourier transform interferometer system," *Appl. optics* **18**, 3404–3420 (1979).
7. T. L. Marshall, C. T. Chaffin, R. M. Hammaker, and W. G. Fateley, "An introduction to open-path FT-IR atmospheric monitoring," *Environ. science & technology* **28**, 224A–232A (1994).
8. S. P. Levine and G. M. Russwurm, "Fourier transform infrared optical remote sensing for monitoring airborne gas and vapor contaminants in the field," *TrAC Trends Anal. Chem.* **13**, 258–262 (1994).
9. L. Shao, W. Wang, P. R. Griffiths, and A. B. Leytem, "Increasing the Quantitative Credibility of Open-Path Fourier Transform Infrared (FT-IR) Spectroscopic Data, with Focus on Several Properties of the Background Spectrum," *Appl. Spectrosc.* **67**, 335–341 (2013).
10. K. C. Cossel, E. M. Waxman, F. R. Giorgetta, M. Cermak, I. R. Coddington, D. Hesselius, S. Ruben, W. C. Swann, G.-W. Truong, G. B. Rieker, and N. R. Newbury, "Open-path dual-comb spectroscopy to an airborne retroreflector," *Optica*. **4**, 724–728 (2017).
11. S. Coburn, C. B. Alden, R. Wright, K. Cossel, E. Baumann, G.-W. Truong, F. Giorgetta, C. Sweeney, N. R. Newbury, K. Prasad, I. Coddington, and G. B. Rieker, "Regional trace-gas source attribution using a field-deployed dual frequency comb spectrometer," *Optica*. **5**, 320 (2018).
12. E. M. Waxman, K. C. Cossel, F. Giorgetta, G.-W. Truong, W. C. Swann, I. Coddington, and N. R. Newbury, "Estimating vehicle carbon dioxide emissions from Boulder, Colorado using horizontal path-integrated column measurements," *Atmospheric Chem. Phys. Discuss.* pp. 1–23 (2018).
13. I. Coddington, N. Newbury, and W. Swann, "Dual-comb spectroscopy," *Optica*. **3**, 414 (2016).
14. G. B. Rieker, F. R. Giorgetta, W. C. Swann, J. Kofler, A. M. Zolot, L. C. Sinclair, E. Baumann, C. Cromer, G. Petron, C. Sweeney, P. P. Tans, I. Coddington, and N. R. Newbury, "Frequency-comb-based remote sensing of greenhouse gases over kilometer air paths," *Optica*. **1**, 290–298 (2014).
15. E. M. Waxman, K. C. Cossel, G.-W. Truong, F. R. Giorgetta, W. C. Swann, S. Coburn, R. J. Wright, G. B. Rieker, I. Coddington, and N. R. Newbury, "Intercomparison of open-path trace gas measurements with two dual-frequency-comb spectrometers," *Atmos. Meas. Tech.* **10**, 3295–3311 (2017).
16. A. Schliesser, N. Picqué, and T. W. Hänsch, "Mid-infrared frequency combs," *Nat. Photonics* **6**, 440–449 (2012).
17. F. Zhu, A. Bicer, R. Askar, J. Bounds, A. A. Kolomenskii, V. Kelessides, M. Amani, and H. A. Schuessler, "Mid-infrared dual frequency comb spectroscopy based on fiber lasers for the detection of methane in ambient air," *Laser Phys. Lett.* **12**, 095701 (2015).
18. Z. Zhang, T. Gardiner, and D. T. Reid, "Mid-infrared dual-comb spectroscopy with an optical parametric oscillator," *Opt. Lett.* **38**, 3148–3150 (2013).
19. M. Yu, Y. Okawachi, A. G. Griffith, N. Picqué, M. Lipson, and A. L. Gaeta, "Silicon-chip-based mid-infrared dual-comb spectroscopy," *Nat. Commun.* **9**, 1869 (2018).
20. Y. Jin, S. M. Cristescu, F. J. M. Harren, and J. Mandon, "Femtosecond optical parametric oscillators toward real-time dual-comb spectroscopy," *Appl. Phys. B* **119**, 1–10 (2015).
21. G. Ycas, F. R. Giorgetta, E. Baumann, I. Coddington, D. Herman, S. A. Diddams, and N. R. Newbury, "High-coherence mid-infrared dual-comb spectroscopy spanning 2.6 to 5.2  $\mu\text{m}$ ," *Nat. Photonics* **12**, 202–208 (2018).
22. A. V. Muraviev, V. O. Smolski, Z. E. Loparo, and K. L. Vodopyanov, "Massively parallel sensing of trace molecules and their isotopologues with broadband subharmonic mid-infrared frequency combs," *Nat. Photonics* **12**, 209 (2018).
23. A. Schliesser, M. Brehm, F. Keilmann, and D. van der Weide, "Frequency-comb infrared spectrometer for rapid, remote chemical sensing," *Opt. Express* **13**, 9029–9038 (2005).
24. P. Jouy, J. M. Wolf, Y. Bidaux, P. Allmendinger, M. Mangold, M. Beck, and J. Faist, "Dual comb operation of  $\lambda \sim 8.2 \mu\text{m}$  quantum cascade laser frequency comb with 1 W optical power," *Appl. Phys. Lett.* **111**, 141102 (2017).
25. O. Kara, L. Maidment, T. Gardiner, P. G. Schunemann, and D. T. Reid, "Dual-comb spectroscopy in the spectral fingerprint region using OPGaP optical parametric oscillators," *Opt. Express* **25**, 32713–32721 (2017).
26. J. Westberg, L. A. Sterczewski, and G. Wysocki, "Mid-infrared multi-heterodyne spectroscopy with phase-locked quantum cascade lasers," *Appl. Phys. Lett.* **110**, 141108 (2017).
27. H. Timmers, A. Kowligy, A. Lind, F. C. Cruz, N. Nader, M. Silfies, G. Ycas, T. K. Allison, P. G. Schunemann, S. B. Papp, and S. A. Diddams, "Molecular fingerprinting with bright, broadband infrared frequency combs," *Optica*. **5**, 727–732 (2018).
28. G.-W. Truong, E. M. Waxman, K. C. Cossel, E. Baumann, A. Klose, F. R. Giorgetta, W. C. Swann, N. R. Newbury, and I. Coddington, "Accurate frequency referencing for fieldable dual-comb spectroscopy," *Opt. Express* **24**, 30495–30504 (2016).
29. I. E. Gordon, L. S. Rothman, C. Hill, R. V. Kochanov, Y. Tan, P. F. Bernath, M. Birk, V. Boudon, A. Campargue, K. V. Chance, B. J. Drouin, J. M. Flaud, R. R. Gamache, J. T. Hodges, D. Jacquemart, V. I. Perevalov, A. Perrin, K. P. Shine, M. A. H. Smith, J. Tennyson, G. C. Toon, H. Tran, V. G. Tyuterev, A. Barbe, A. G. Császár, V. M. Devi, T. Furtenbacher, J. J. Harrison, J. M. Hartmann, A. Jolly, T. J. Johnson, T. Karman, I. Kleiner, A. A. Kyuberis, J. Loos, O. M. Lyulin, S. T. Massie, S. N. Mikhailenko, N. Moazzen-Ahmadi, H. S. P. Müller, O. V. Naumenko, A. V. Nikitin, O. L. Polyansky, M. Rey, M. Rotger, S. W. Sharpe, K. Sung, E. Starikova, S. A. Tashkun, J. V. Auwera, G. Wagner, J. Wilzewski, P. Wcislo, S. Yu, and E. J. Zak, "The HITRAN2016 molecular spectroscopic database," *J. Quant. Spectrosc. Radiat. Transf.* **203**, 3–69 (2017).
30. S. W. Sharpe, T. J. Johnson, R. L. Sams, P. M. Chu, G. C. Rhoderick, and P. A. Johnson, "Gas-Phase Databases for Quantitative Infrared Spectroscopy," *Appl. Spectrosc.* **58**, 1452–1461 (2004).
31. C. D. Boone, K. A. Walker, and P. F. Bernath, "Speed-dependent Voigt profile for water vapor in infrared remote sensing applications," *J. Quant. Spectrosc. Radiat. Transf.* **105**, 525–532 (2007).